Understanding the Chemical Contribution to the Enhancement Mechanism in SERS: Connection with Hammett Parameters

Dhara J. Trivedi [†, *], *Brendan Barrow*[†], *and George C. Schatz*[‡]

[†] Department of Physics, Clarkson University, 8 Clarkson Ave., Potsdam, New York 13699, United States

[‡] Department of Chemistry, Northwestern University, 2145 Sheridan Road, Evanston, Illinois 60208, United States

KEYWORDS: Spectroscopy, Raman Spectra, Surface enhanced Raman scattering, Plasmon

*Corresponding author: dtrivedi@clarkson.edu

ABSTRACT: The enhancement mechanism due to the molecule-surface chemical interaction in surface-enhanced Raman scattering (SERS) has been characterized using a theoretical approach based on time dependent density functional theory. This includes a systematic study of the chemical mechanism (CM) to the SERS enhancement for halogen substituted benzenethiols interacting with a silver cluster. Changing the halogen on benzenethiol enables us to systematically modulate interactions between the benzenethiol ring and the metal cluster. We observe a decrease in the CM enhancement factor with an increase in atomic number of the halogen for *para*- substitutions. For *meta*- substitutions, there is no such trend. However, the results scale linearly with the Hammett parameters for both *meta* and *para* halogens, which provides an important predictive tool for interpreting chemical enhancements. We also study the effect of solvation on the CM, showing that there is a systematic increase in enhancement with increasing solvent dielectric constant. The correlation of CM with other properties, such as the amount of charge transfer between adsorbate and metal, or the excitation energies of charge transfer states, is much less predictive than the Hammett parameter correlation.

1 Introduction

Raman spectroscopy is a powerful technique for determining structural information about a molecular system. This inherently weak process is greatly enhanced when molecules are adsorbed onto noble-metal nanoparticles, leading to surface-enhanced Raman scattering (SERS).[1–5] The electromagnetic field generated due to excitation of localized surface plasmon resonance in these metal nanostructures can typically lead to 10^5 – 10^8 enhancements of the Raman cross sections.[6–10] In recent years, SERS has been transformed into a robust single molecule technique[11–15] due to advances in nanofabrication[16–21] combined with an increased understanding of the plasmonic properties of nanomaterials.[22–25] This technique has found a wide range of applications in ultra-sensitive chemical and biological sensing, environmental analysis, and surface science.[12,26,27]

Although SERS was discovered over 40 years ago,[1–3] the complete picture of the enhancement mechanism remains an active area of research. Away from molecular resonances, there are two primary contributors to the enhancement mechanism: the electromagnetic (EM) enhancement and the chemical mechanism (CM). The EM enhancement (Fig. 1a), which often dominates, is caused by the strong local field induced by the incident light at the molecule's position because of plasmon excitation in the metallic nanoparticle.[5,8,10,28] The CM enhancement is postulated to arise from two distinct processes: 1) enhancement due to nonresonant changes in the molecular polarizability that occur upon absorption of the molecule on the nanoparticle (Fig. 1b), and 2) charge transfer (CT) resonance enhancement (Fig. 1c) when the excitation wavelength is resonant with molecule-nanoparticle CT transitions.[5,29,30] There can also be resonant Raman

excitation associated with a molecular electronic excitation (Fig. 1d), often referred to as a surface enhanced resonance Raman scattering (SERRS).[5,6] Although we prefer to discuss the enhancement mechanisms separately, it is important to realize that all these enhancements are not independent of each other, and there may be specific wavelengths where each one dominates.

The contribution of the CM mechanism to SERS is still open for discussion,[31] which provides motivation for further investigation of the CM. Theoretical studies of the optical properties on the atomistic scale for molecule-metal complexes can provide key insights into the nature and strength of the bonds between the molecule and nanoparticle, the effect of the excitation wavelength, and the factors that determine large enhancements. In particular, quantum mechanical approaches have shown good ability to describe CM enhancements for small Ag and Au clusters interacting with molecules like pyridine or benzenethiol,[32] using a model in which the metal particle is replaced by Ag or Au clusters with 10-100 atoms. Further, Jensen et al.[33,34] developed a time-dependent density functional theory (TDDFT) methods for calculating frequency-dependent polarizability derivatives with this molecule/cluster model, and successfully used this to model SERS spectra. Subsequently, Morton and Jensen[35] proposed that the static polarizability derivatives from these calculations provide a useful measure of the chemical effect, and Valley et al[32] showed that the predictions of this approach match well with experimental results. This provides a key link for using theory to understand the CM.

Functional groups on adsorbed molecules allow for systematic variation of the direct chemical interaction between molecule and metal cluster.[35] In particular, halogen substituents are known to show a linear trend in reactivity and bond energy moving from top to bottom in the periodic

table.[36] This trend can be quantified using empirical parameters known as the Hammett parameters.[36,37] There have been extensive studies over the years of these parameters,[37] and in general they have been associated with a combination of inductive and resonance (sometimes called mesomeric) effects, where inductive effects are related to the electronegativity of the halogen, and the resonance effects to participation of the halogen orbitals in bonding with the π orbitals on the adjacent benzene ring. The connection of Hammett parameters with SERS is unknown.

In this paper, we present a systematic study of the chemical EFs in the SERS spectra of halogenated benzenethiol derivatives, for meta and para substitution, both in vacuum and in ethanol solvent environment. We study the correlation of the CM enhancements with a number of properties of the molecule, including ground state properties like the amount of charge transfer between metal and molecule, and excited state properties such as the frequency of resonant CT excitations. Overall we find that the strongest correlation is with the Hammett parameters. This investigation thus provides important microscopic insight concerning factors that contribute to SERS enhancement phenomena.

2 Computational Methodology

Normal Raman scattering (NRS) and SERS spectra are computed using TDDFT, where we determine the frequency-dependent polarizability from the first-order change in the electronic density in the presence of an applied field. We use a cluster model to mimic the SERS spectra, following the work of Valley et al[32] in which a Ag_{19}-thiolate complex is constructed, starting with a tetrahedral Ag_{20} cluster, and removing the vertex atom opposite to the thiolate adsorption

site. Note that this produces a closed-shell structure, which greatly simplifies the calculations. All calculations were done using the Amsterdam Density Functional ADF program package,[38–40] and the impact of the solvent on spectra and in turn EFs was also studied using the Conductor like Screening Model (COSMO)[41–43] that is contained in ADF.

2.1 Computational Details

The Becke-Perdew (BP86) exchange-correlation functional[44,45] and a triple-ζ polarized (TZP) Slater-type basis set from the ADF library were used. Full geometry optimization for isolated molecule and molecule-cluster complex was done with a frozen-core approximation, with the 1s-4p core kept frozen for Ag. Scalar relativistic effects were included using the zeroth-order regular approximation (ZORA).[46] The vibrational frequencies and normal modes were calculated numerically, within the harmonic approximation, where the BP86 functional results in harmonic frequencies of small molecules close to experimental results without the use of scaling factors.[47] The polarizability derivatives were then calculated by numerical three-point differentiation with respect to the normal mode displacements[48] using the AOResponse[33,34] module implemented in ADF. This allows us to selectively study the Raman intensities of the normal modes associated with the adsorbed molecules. Absolute Raman intensities are presented here in terms of the differential Raman scattering cross section. For Stokes scattering with an experimental setup having a 90° scattering angle and perpendicular plane-polarized light, the cross section is given by,[49]

$$\frac{d\sigma}{d\Omega} = \frac{\pi^2}{\epsilon_0^2}\left(\tilde{\upsilon}_{in} - \tilde{\upsilon}_p\right)^4 \frac{h}{8\pi^2 c\tilde{\upsilon}_p}\left[45\overline{\alpha}'^2_p + 7\gamma'^2_p\right] \times \frac{1}{45\left[1 - \exp\left(-hc\tilde{\upsilon}_p/k_B T\right)\right]} \quad (1)$$

where $\tilde{\upsilon}_{in}$, $\tilde{\upsilon}_p$ are the frequencies of the incident light and of pth vibrational mode, respectively. $\bar{\alpha}'_p$ and γ'_p are the isotropic and anisotropic polarizability derivatives with respect to vibrational mode p. The electronic polarizabilities have been calculated via TDDFT and with an excited state lifetime of Γ = 0.1 eV. This is the same value used in earlier work[50] and leads to an excited state width that is similar to the plasmon width based on commonly used Drude function for silver. For such a small molecule this orientation averaged cross sections generates more reliable results due to random flopping motion,[51] unlike big flat molecules.[52]

We used a wavelength of 633 nm (1.96 eV) for these calculations, which avoids the effects of resonance enhancement,[53] both of the plasmon and of the molecule, on the Raman cross sections (Eq 1), making the results suitable for characterizing the chemical mechanism based on earlier studies.[32,35] The integrated enhancement factors are computed by the ratio of the sum of the intensities,[32]

$$EF = \frac{I^{tot}_{Ag_{19}-molec}}{I^{tot}_{molec}} = \frac{\sum_m I^m_{Ag_{19}-molec}}{\sum_n I^n_{molec}} \quad (2)$$

where $I^m_{Ag_{19}-mole}$ is the differential Raman cross-section for the mth vibrational mode of the Ag_{19}-molecule complex, and correspondingly I^n_{mole} is the differential Raman cross-section for the nth vibrational mode of the isolated benzenethiol molecule.

Since most of the experiments are conducted in a solvent, we also computed the EFs using the ADF-COSMO[38] approach. The solvent ethanol was utilized in order to incorporate solvatochromic shifts into the results.[54]

3 Results and Discussion

To investigate the influence of functional groups on enhancement factors, halogen substituted benzenethiols (namely, fluoride, chloride, bromide, and iodine functionalized benzenethiols) were studied theoretically using silver substrates. Since the *ortho*-position introduces steric hindrance and some surface-binding difficulties,[55] only the *para*- and *meta*-positions were considered for the substitution. Figure 2 is an illustration of the metal – molecule complex with the position of the functional group indicated. The optimized structure of the Ag_{19}-thiolate complex has the sulfur binding with two silver atoms of the cluster (Fig. 2 (a)). We only changed functional groups on the benzenethiol to obtain all other required complexes and to optimize them. Using the AOResponse module we then obtained the 633 nm polarizabilities, which were used to obtain the Raman intensities.

To understand the influence of modified electronic interactions that occur due to the influence of the halogen functional groups on the enhancement factors we first consider the enhancements for the set of peaks occurring only at ~1600 cm^{-1}. This single peak analysis has been implemented previously[32] and it is useful for this class of molecules, as the peak is present in all the scenarios we need (SERS and NRS spectra) for all the halogenated aromatic molecules. Typically, the C-C stretching mode of the ring near 1570 cm^{-1} is doubly degenerate and shows large shifts depending on the halogen. Table 1 lists normal modes occurring near ~1600 cm^{-1} for

benzenethiol and the Ag- benzenethiol complex, in vacuum and solvent. The vibrational modes between 500 and 3000 cm^{-1} for these structures are also listed in the Table 1 for a detailed review. The mode near ~2600 cm^{-1}, due to the S-H bond stretching, is present only in the free molecule since we are assuming a thiolate forms on the surface. The effect of the functional group on the peaks occurring around ~1600 cm^{-1} can be found in the Supporting Information. It can be seen that the shifts and splits in these degenerate peaks depend on the position of the functional group. This directly displays distinct interactions depending on the position of functionalization. In 1975, a detailed experimental investigation of fundamental frequencies involved in NRS spectra indicated a systematic shift with choice of halogen.[56] Our calculations show that such characteristics are preserved in the SERS spectra.

EFs for the set of peaks occurring at 1600 cm^{-1} for each of the benzenethiol derivatives as determined from TDDFT calculations, are shown in Table 2, and are plotted in Fig. 3. The results show a decrease in the EFs going down the periodic table for *para*- substitutions but varying results for *meta*- substitutions, with bromine having the highest EF. In the presence of the solvent, the EFs are much higher than the values of those in vacuum, which can be attributed to larger dipole and smaller excitation energies for charge transfer transitions (further analysis is given below), as arises from solvatochromic shifts induced by the solvent medium.[57,58] Results for unsubstituted benzenethiol (labelled H) are also included in Fig. 3, and we see that these are close to those for m-F both in vacuum and in solvent.

To examine differences between the results, EFs are also calculated using the full range of peaks between 500 and 2000 cm^{-1}. Since the peak between 2000 cm^{-1} and 3000 cm^{-1} is only due to S-H

bond vibrations, we excluded this in the full range calculations. These results, which are presented in Tables 3 (vacuum) and 4 (solvent), also show preservation of the trends seen for peaks around 1600 cm^{-1}, further validating the selective peak analysis. In the following sections we examine these results in detail.

3.1 Correlation with electronic properties

To investigate the correlation between EFs and electronic properties, we examine several characteristics of the metal-molecule complexes. Table 3 lists the EFs, the HOMO-LUMO gap, the energy of the lowest orbital with strong (>20%) CT character, the ground state charge transfer q_e between the metal cluster and molecule, and the lowest energy CT excitation energy (either to Ag or from Ag) for each molecule/cluster studied in vacuum. Table 4 gives the corresponding results in ethanol solvent. The Tables show that the bandgap is not strongly influenced by halogen or solvent, as makes sense since the bandgap corresponds to a transition between states of the metal cluster that are primarily in the core of the cluster and therefore not sensitive to these substitutions.

Concerning the lowest orbital with strong CT character, we note that for each complex the interaction energy between molecule and metal cluster can be decomposed into three contributions.[59]: 1) the classical electrostatic interaction between the unperturbed charge distributions of both systems, 2) the Pauli repulsion interaction between occupied orbitals, and 3) the interaction between occupied and virtual orbitals, which leads to ground state charge transfer (GS-CT).[40] The analysis of molecular orbital mixing can reveal the energies at which such GS-

CT occurs.[60] Such GS-CT leads to mixing of metal molecular orbitals, which can be extracted from the optimization calculation. As shown in Table 3 the mixing occurs at less negative energies for both *para-* and *meta-* positions as we go down the periodic table, which means that the more electronegative fluorine leads to more stable orbitals with significant CT character than the other halogens. In the presence of solvent (Table 4), the orbital energy for >20% mixing is often less negative (meaning less stable) than in vacuum, suggesting that there is screening of charges by the solvent, which destabilizes these states. However not all the trends are consistent for the heavier halogens in solvent.

Tables 3 and 4 show that q_e is negative for all the cases studied, meaning that there is net charge flowing to the molecule. The values only slightly change with changing halogen, which indicates that the dominant effects dictating ground state charge transfer are not related to the halogens.

3.2 CT Excited State

In order to explore the possible contribution of CT states, we used TDDFT to compute excited states for each molecule-metal complex.[61] Using the iterative Davidson method, the lowest 200 singlet excitation energies were calculated. The charge transfer characteristics were extracted from the computed excited states, using simple python scripts available in the Schatz's group. This calculation yields the energies of states with the charge transfer capacities in both directions, from molecule to Ag_{19} cluster and vice versa. Table 3 shows that in vacuum the CT levels from molecule to metal redshift for both meta and para with increase in atomic number of the substituted halogens; conversely, Table 4 shows that in the presence of solvent this trend is

lost due to solvatochromic shifts.[62] Depending on the individual systems the solvent effects significantly impact excited states and bond-order alternation of them.[63] The CT excitation energies are typically in the range 3.2-3.5 eV in Table 3, with values that aren't much different for the "to Ag" and "from Ag" cases. These energies are smaller in Table 4, with values in the range 2.5-3.2 eV. These smaller values are consistent with expectations associated with the solvochromic effect for charge transfer transitions. However, the variation of these energies with halogen is nonsystematic. This is an important result, as argues against excited state charge transfer resonances as dominating the chemical effect.

3.3 Hammett Parameters

To correlate and benchmark the EFs for the various benzenethiols, we examined correlation with the Hammett parameters.[36,37] These parameters were originally developed to empirically describe the electronic effect of functional groups on the reactivity of benzene rings, and the results are known to depend on both inductive effects and a resonance (mesomeric) effects.[64] Relative to a hydrogen atom functional group (e.g., benzenethiol), the effects of functional groups at the *para*- and *meta*- positions of the substituted benzenethiols on reactivity can be characterized quantitatively using the Hammett parameters. However, the connection of these parameters with SERS intensities is unknown. In Figure 4, we show the total EF plotted against the Hammett constants for the different functional groups.[65] It is immediately evident that there is a clear linear correlation between EFs and Hammett parameters depending on the site of functionalization, and this correlation works equally well for the vacuum and solvent results in Figure 4. For the meta position, the EFs increase linearly with the Hammett parameter going down the periodic table, while for para substitution the trend reverses. The reason behind such a

reversing trend is the site dependent characteristics of the halogens. The halogens have both withdrawing character (induction) due to electronegativity, and donor character (mesomerism or resonance) due to resonance involving lone electron pairs on the halogens interacting with π-orbitals on the benzene ring. The induction characteristic is more prominent with the halogen functional in the *meta-* position. The presence of the solvent increases the inductive effect, leading to the highest correlation between the Hammett parameters and EFs. On the contrary, the mesomeric characteristic is more prominent for *para-* substitutions. The fluorine derivative has the highest mesomeric characteristic[66,67] among halogen derivatives[68] and, it is the most important correlation with the high EF in 4-fluorobenzenethiol. Of the curves in Figs. 3 and 4, the results for iodine show the largest discrepancies from linearity. While the deviations from linearity are not especially worse than are found in other applications of the Hammett parameters,[69,70] studies that include iodine are unusual, so it is hard to know if this represents a systematic trend. Even though, the data used for Figs 3 and 4 are from the partial peak analysis (Table 2) the full range integrated EFs (Table 3 and Table 4) follows the identical trend. We did not include the unsubstituted benzenethiol results in from Fig. 3 in Fig. 4, but if we had included these results, which correspond to a Hammett parameter of zero, they are not on the linear portions of these plots. This shows a limitation of the Hammett correlation that should be considered in further work.

4 Conclusions

To recapitulate, we presented a systematic study of the non-resonant enhancement factors of benzenethiol derivatives interacting with a small silver cluster (Ag_{19}) using TDDFT, with the goal of using such calculations to provide microscopic insight into the SERS enhancement

mechanisms. By methodically substituting the halogen functional groups in *para*- and *meta*-positions on the thiophenol, the metal – molecule interactions can be altered in a controlled manner. Surprisingly, the calculated EFs do not have similar trends for both positions. Instead, we find that *meta*- functionalization leads to enhancement factors that vary smoothly down the periodic table, following the electronegative properties of the halogen group, while *para*-substitution of the functional groups leads to complex interaction with the benzene ring electrons, which causes reordering of enhancement factors. The mechanism that controls this trend is complex and most likely not driven by a single property. We examined various measures of charge transfer in the ground state, and concerning low lying excited states, but in all cases, these do not capture the trends that we see. However, the results correlate quite well with the Hammett parameters, so inductive and mesomeric effects are key factors in governing enhancements. We are not aware of experimental results for benzene thiolates or other molecules that would enable us to verify this prediction, but given that the CM enhancement calculations we have performed are similar to what has been used previously for other molecules where theory and experiment were in good agreement, we feel our prediction concerning the Hammett parameters is an important guide to future experimental studies. Another prediction from this work is that the presence of solvent leads to noticeable increase in the chemical enhancement factor. While the role of solvent dielectric on the Raman intensities of small molecules in vacuum and solution been studied theoretically, and it is known that the intensities are factors of ~2 higher in solution,[71] solvent effects on the CM have not been considered, so this is a second prediction worthy of experimental studies.

Supporting Information

Theoretical details about optimized geometries of the benzenethiol and Ag- benzenethiol complex, details regarding vibrational frequencies around 1600 cm^{-1} along with SERS spectra for all halogen derivatives of benzenethiol and its metal-molecule complex. Additionally, the studies considered binding energies for all metal-molecule complexes and the correlation with Hammett parameters.

Acknowledgments

This work is dedicated to all inspiring role models, mentors, and collaborators (like Prof. Teri W. Odom, Prof. Anna I. Krylov, Prof. Svetlana V. Kilina, and Prof. Silvana Andreescu). Their groundbreaking scientific contributions and mentoring have inspired many students, including the authors. Their research creativity has contributed to many different phases of physical chemistry and have impacted the scientific community at large. This research was sponsored by the National Science Foundation under Grant No. CHE-1760537.

Data Availability Statement

The data that support the findings of this study are available within the article.

References

[1] M. Fleischmann, P.J. Hendra, and A.J. McQuillan, Chem. Phys. Lett. **26**, 163 (1974).

[2] D.L. Jeanmaire and R.P. Van Duyne, J. Electroanal. Chem. **84**, 1 (1977).

[3] M.G. Albrecht and J.A. Creighton, J. Am. Chem. Soc. **99**, 5215 (1977).

[4] L. Jensen, C.M. Aikens, and G.C. Schatz, Chem. Soc. Rev. **37**, 1061 (2008).

[5] M. Moskovits, Rev. Mod. Phys. **57**, 783 (1985).

[6] S. Nie and S. Emory, Science **275**, 1102 (1997).

[7] K. Kneipp, Y. Wang, H. Kneipp, L.T. Perelman, I. Itzkan, R.R. Dasari, and M.S. Feld, Phys. Rev. Lett. **78**, 1667 (1997).

[8] G.C. Schatz, M.A. Young, and R.P. Van Duyne, in *Surface-Enhanced Raman Scatt.* (Springer, 2006), pp. 19–45.

[9] S. Zou and G.C. Schatz, Chem. Phys. Lett. **403**, 62 (2005).

[10] J. Gersten and A. Nitzan, J. Chem. Phys. **73**, 3023 (1980).

[11] K. Kneipp, H. Kneipp, I. Itzkan, R.R. Dasari, and M.S. Feld, Chem. Rev. **99**, 2957 (1999).

[12] C.R. Yonzon, C.L. Haynes, X. Zhang, Walsh Joseph T., and R.P. Van Duyne, Anal. Chem. **76**, 78 (2004).

[13] D.A. Schultz, Curr. Opin. Biotechnol. **14**, 13 (2003).

[14] Y.C. Cao, R. Jin, and C.A. Mirkin, Science **297**, 1536 LP (2002).

[15] J.N. Anker, W.P. Hall, O. Lyandres, N.C. Shah, J. Zhao, and R.P. Van Duyne, Nat Mater **7**, 442 (2008).

[16] Y. Xia and N.J. Halas, MRS Bull. **30**, 338 (2005).

[17] C.J. Murphy, T.K. Sau, A.M. Gole, C.J. Orendorff, J. Gao, L. Gou, S.E. Hunyadi, and T. Li, J. Phys. Chem. B **109**, 13857 (2005).

[18] B.D. Gates, Q. Xu, M. Stewart, D. Ryan, C.G. Willson, and G.M. Whitesides, Chem. Rev. **105**, 1171 (2005).

[19] J. Henzie, J.E. Barton, C.L. Stender, and T.W. Odom, Acc. Chem. Res. **39**, 249 (2006).

[20] P.D. Jadzinsky, G. Calero, C.J. Ackerson, D.A. Bushnell, and R.D. Kornberg, Science **318**, 430 LP (2007).

[21] K. Chandra, B.K. Rugg, M.A. Ratner, M.R. Wasielewski, and T.W. Odom, J. Am. Chem. Soc.

140, 3219 (2018).

[22] W. Yang, G.C. Schatz, and R.P. Van Duyne, J. Chem. Phys. **103**, 869 (1995).

[23] K.L. Kelly, E. Coronado, L.L. Zhao, and G.C. Schatz, J. Phys. Chem. B **107**, 668 (2003).

[24] E. Prodan, C. Radloff, N.J. Halas, and P. Nordlander, Science **302**, 419 (2003).

[25] H. Wang, D.W. Brandl, P. Nordlander, and N.J. Halas, Acc. Chem. Res. **40**, 53 (2007).

[26] C.A. Mirkin, R.L. Letsinger, R.C. Mucic, and J.J. Storhoff, Nature **382**, 607 (1996).

[27] A.J. Haes, W.P. Hall, L. Chang, W.L. Klein, and R.P. Van Duyne, Nano Lett. **4**, 1029 (2004).

[28] K.A. Willets and R.P. Van Duyne, Annu. Rev. Phys. Chem. **58**, 267 (2007).

[29] A. Campion and P. Kambhampati, Chem. Soc. Rev. **27**, 241 (1998).

[30] S.M. Morton, D.W. Silverstein, and L. Jensen, Chem. Rev. **111**, 3962 (2011).

[31] M. Moskovits, Phys. Chem. Chem. Phys. **15**, 5301 (2013).

[32] N. Valley, N. Greeneltch, R.P. Van Duyne, and G.C. Schatz, J. Phys. Chem. Lett. **4**, 2599 (2013).

[33] L. Jensen, J. Autschbach, and G.C. Schatz, J. Chem. Phys. **122**, (2005).

[34] L. Jensen, L.L. Zhao, J. Autschbach, and G.C. Schatz, J. Chem. Phys. **123**, 174110 (2005).

[35] S.M. Morton and L. Jensen, J. Am. Chem. Soc. **131**, 4090 (2009).

[36] L.P. Hammett, J. Am. Chem. Soc. **59**, 96 (1937).

[37] C. Hansch, A. Leo, and R.W. Taft, Chem. Rev. **91**, 165 (1991).

[38] C.C. Pye and T. Ziegler, Theor. Chem. Acc. **101**, 396 (1999).

[39] E.J. Baerends, J. Autschbach, A. Bérces, C. Bo, P.M. Boerrigter, L. Cavallo, D.P. Chong, L. Deng, R.M. Dickson, and D.E. Ellis, Theor. Chem. Vrije Univ. Amsterdam, URL Http//Www. Scm. Com **42**, (2006).

[40] G. t Te Velde, F.M. Bickelhaupt, E.J. Baerends, C. Fonseca Guerra, S.J.A. Van Ginsbergen,

J.G. Snijders, T. Ziegler, S.J.A. van Gisbergen, J.G. Snijders, and T. Ziegler, J. Comput. Chem. **22**, 931 (2001).

[41] A. Klamt and G. Schüürmann, J. Chem. Soc. Perkin Trans. 2 799 (1993).

[42] A. Klamt, *Conductor-like Screening Model for Real Solvents: A New Approach to the Quantitative Calculation of Solvation Phenomena Starting from the Question of Why Dielectric Continuum Models Give a Fairly Good Description of Molecules* (1995).

[43] A. Klamt and V. Jonas, J. Chem. Phys. **105**, 9972 (1996).

[44] A.D. Becke, Phys. Rev. A **38**, 3098 (1988).

[45] J.P. Perdew, Phys. Rev. B **33**, 8822 (1986).

[46] E. van Lenthe, J.G. Snijders, and E.J. Baerends, J. Chem. Phys. **105**, 6505 (1996).

[47] J. Neugebauer and B.A. Hess, J. Chem. Phys. **118**, 7215 (2003).

[48] M. Reiher, J. Neugebauer, and B.A. Hess, Zeitschrift Für Phys. Chemie **217**, 91 (2003).

[49] J. Neugebauer, M. Reiher, C. Kind, and B.A. Hess, J. Comput. Chem. **23**, 895 (2002).

[50] Zhao, L. Jensen, and G.C. Schatz, J. Am. Chem. Soc. **128**, 2911 (2006).

[51] G.C. Schatz and N.A. Valley, in *Front. Surface-Enhanced Raman Scatt.* (2014), pp. 1–17.

[52] N. Jiang, N. Chiang, L. R. Madison, E. A. Pozzi, M. R. Wasielewski, T. Seideman, M. A. Ratner, M. C. Hersam, G. C. Schatz, and R. P. Van Duyne, Nano Lett. **16**, 3898 (2016).

[53] S.K. Saikin, R. Olivares-Amaya, D. Rappoport, M. Stopa, and A. Aspuru-Guzik, Phys. Chem. Chem. Phys. **11**, 9401 (2009).

[54] C.K. Wang, Y.H. Wang, Y. Su, and Y. Luo, J. Chem. Phys. **119**, 4409 (2003).

[55] C.S. Allen and R.P. Van Duyne, Chem. Phys. Lett. **63**, 455 (1979).

[56] T. H., B. J.-L., H. I., and S. T., J. Raman Spectrosc. **4**, 235 (1975).

[57] R. Rudyk, M.A.A. Molina, M.I. Gómez, S.E. Blanco, and F.H. Ferretti, J. Mol. Struct.

THEOCHEM **674**, 7 (2004).

[58] R.L. Gieseking, M.A. Ratner, and G.C. Schatz, J. Phys. Chem. A **120**, 9878 (2016).

[59] F.M. Bickelhaupt and E.J. Baerends, Rev. Comput. Chem. **15**, 1 (2000).

[60] G. Sini, J.S. Sears, and J.L. Brédas, J. Chem. Theory Comput. **7**, 602 (2011).

[61] F.C. Grozema, R. Telesca, H.T. Jonkman, L.D.A. Siebbeles, and J.G. Snijders, J. Chem. Phys. **115**, 10014 (2001).

[62] M. Pápai, M. Abedi, G. Levi, E. Biasin, M.M. Nielsen, and K.B. Møller, J. Phys. Chem. C **123**, 2056 (2019).

[63] P. Suppan, J. Photochem. Photobiol. A Chem. **50**, 293 (1990).

[64] H. Szatylowicz, A. Jezuita, T. Siodla, K.S. Varaksin, M.A. Domanski, K. Ejsmont, and T.M. Krygowski, ACS Omega **2**, 7163 (2017).

[65] E. Leffler, J.E.; Grunwald, *Table 7.1."Hammett Substituent Constants, σ, Based on the Ionization of Benzoic Acids"* (1963).

[66] X. Difluoride, P. Vi, and P. Vi, Natl. Sci. Found. 1 (2017).

[67] T. Yang, L. Huang, C. Xiao, J. Chen, T. Wang, D. Dai, F. Lique, M.H. Alexander, Z. Sun, D.H. Zhang, X. Yang, and D.M. Neumark, Nat. Chem. **11**, 744 (2019).

[68] D.T. Clark, J.N. Murrell, and J.M. Tedder, J. Chem. Soc. 1250 (1963).

[69] C. Hansch, A. Leo, and R. W. Taft, Chem. Rev. **91**, 165 (1991).

[70] Wikipedia contributors, Wikipedia, Free Encycl. Hammett Equation (2020).

[71] C. Cappelli, S. Corni, and J. Tomasi, J. Chem. Phys. **115**, 5531 (2001).

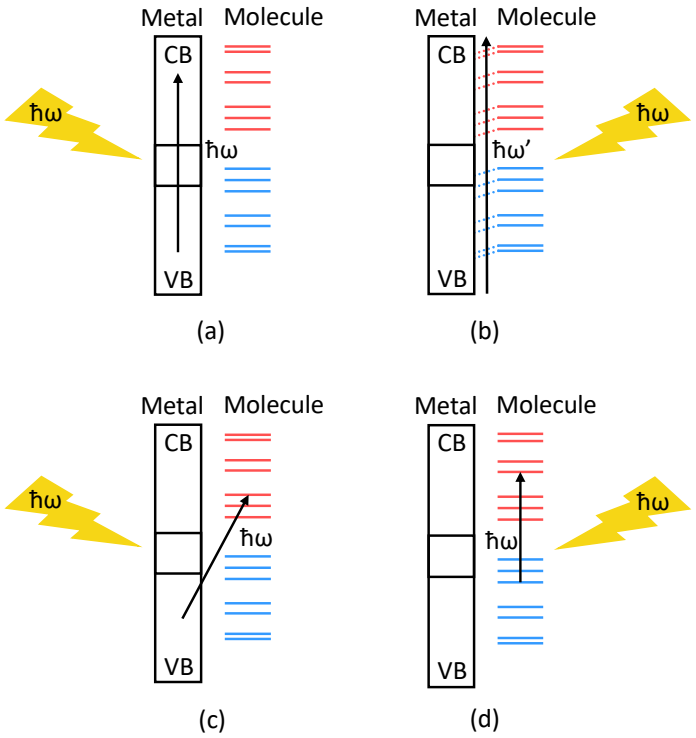

Figure 1: Schematic diagram of the enhancement mechanisms of the Raman spectra: (a) Plasmon resonance enhancement, (b) Chemical enhancement, (c) Charge transfer enhancement, and (d) Resonance Raman enhancement. Solid red lines are unoccupied molecular orbitals, blue lines occupied molecular orbitals.

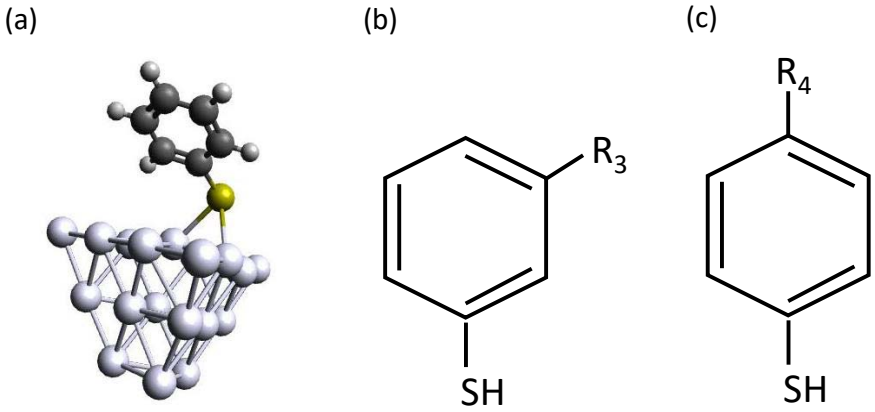

Figure 2: (a) Configuration of Ag_{19}-Benzenethiol complex. (b) Benzenethiol with *meta*-substitution and (c) Benzenethiol with para- substitution.

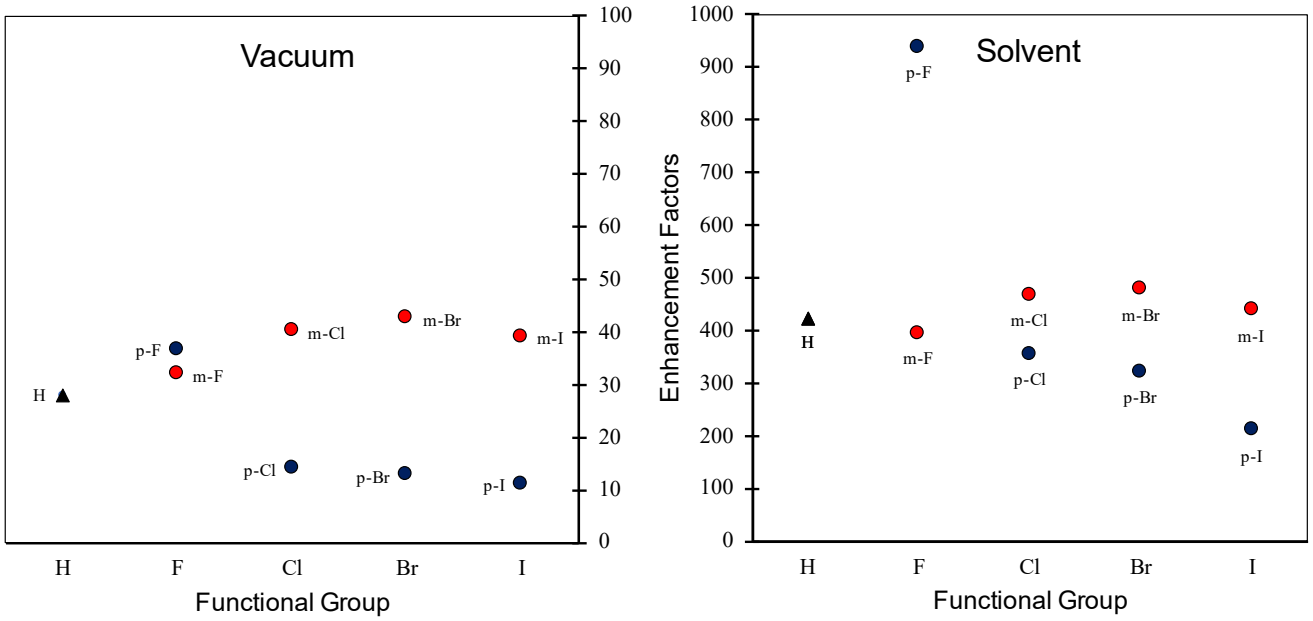

Figure 3: Correlation between the enhancement factors and the period of the periodic table. The EF values reported corresponds to the enhancements calculated using the singlet or doublet peaks found ~1600 cm^{-1}.

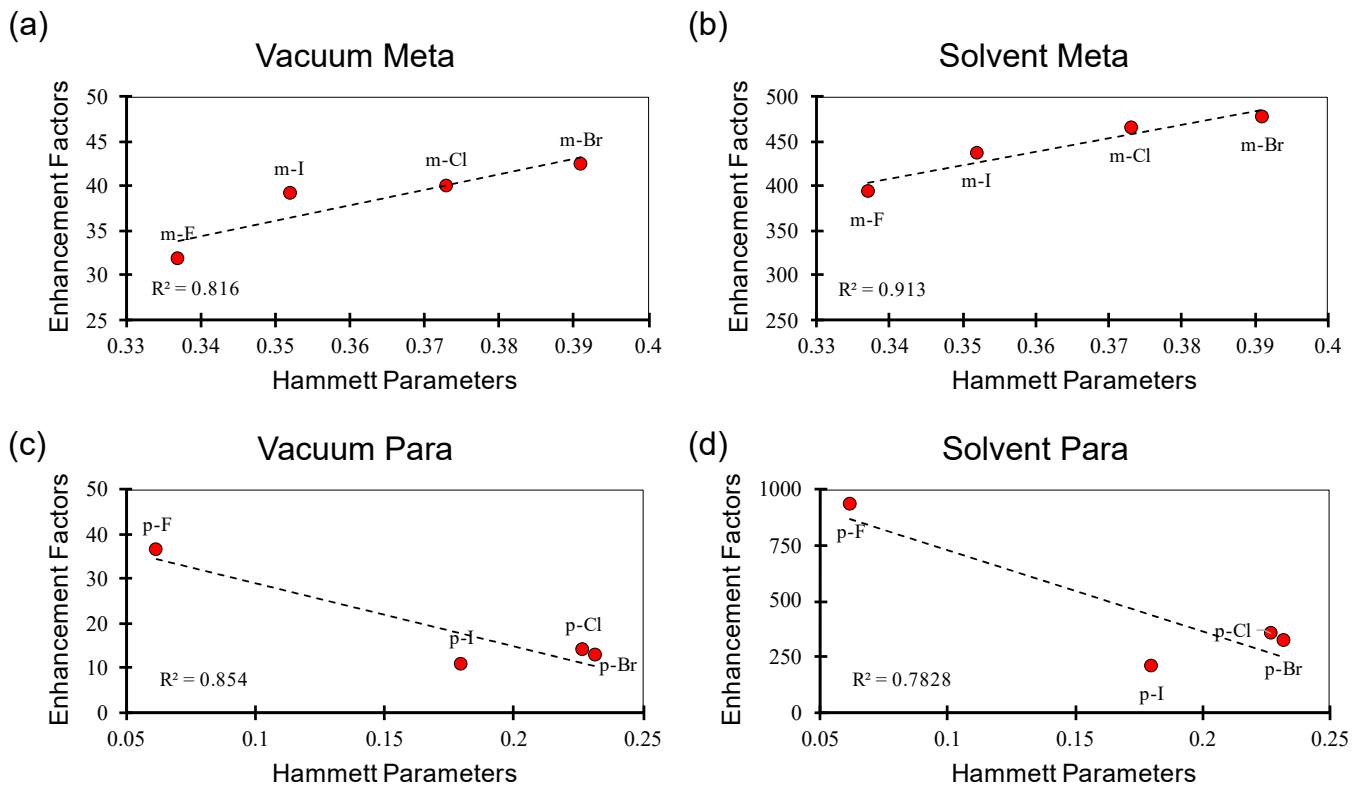

Figure 4: Comparison of the enhancement factors with associated Hammett parameters for each halogen substitution on Benzenethiol. The EF values reported corresponds to the enhancements calculated using the singlet or doublet peaks found ~1600 cm^{-1}.

Table 1: Vibrational Mode Energies for Benzenethiol (BT) and Ag_{19}-Benzenethiol Complex

Vacuum		Solvent	
BT (cm^{-1})	Ag-BT (cm^{-1})	BT (cm^{-1})	Ag-BT (cm^{-1})
614.4	609.2	610.3	605.7
681.8	677.4	680.5	675.5
688.2	686.3	683.1	684.2
721.9	722.9	720.0	718.1
809.2	819.5	809.3	815.7
870.8	876.8	872.2	875.3
896.9	942.2	883.7	942.2
939.9	964.6	940.2	963.5
961.7	982.6	959.4	979.2
989.2	1012.7	984.4	1008.3
1019.8	1047.8	1013.5	1046.1
1072.8	1059.8	1065.6	1057.2
1081.5	1145.2	1073.2	1134.9
1149.9	1160.3	1137.4	1151.9
1170.1	1270.8	1159.3	1269.0
1297.6	1312.5	1293.6	1309.9
1324.6	1415.2	1318.8	1410.9
1430.3	1444.1	1423.9	1441.2
1462.4	1543.7	1456.3	1541.1
1565.5	1558.1	1559.3	1552.9
1577.0		1567.7	
2611.0		2611.1	

Table 2: Partial enhancement factors (peak at 1600 cm^{-1}) for halogen substitutions on benzenethiol in vacuum and solvent

Functional Group	*Vacuum*	*Solvent*
m-F	31.9	393.1
m-Cl	40.1	465.7
m-Br	42.4	476.9
m-I	39.1	437.5
p-F	36.6	937.0
p-Cl	13.9	353.3
p-Br	12.8	320.4
p-I	11.0	209.2
H	28.1	423.4

Table 3: Theoretical data including enhancement factors (EF) and properties of charge transfer (CT) states from calculations performed for halogen substitutions on benzenethiol in vacuum

Functional Group	*Total EF (peaks between 500- 2000 cm^{-1})*	*HOMO-LUMO gap (eV)*	*Lowest CT Orbital (with 20% mixing) (eV)*	*Molecule Charge (q_e)*	*CT State peak (eV)*	
					To Ag	*From Ag*
m-F	24.8	0.78	-6.79	-0.234	3.32	3.18
m-Cl	28.1	0.78	-6.76	-0.243	3.28	3.42
m-Br	28.6	0.78	-6.73	-0.244	3.20	3.32
m-I	25.2	0.78	-6.69	-0.243	3.16	3.36
p-F	23.8	0.78	-6.99	-0.228	3.52	3.34
p-Cl	13.6	0.77	-6.91	-0.239	3.28	3.56
p-Br	12.6	0.77	-6.89	-0.239	3.28	3.44
p-I	10.0	0.77	-6.76	-0.238	3.22	3.42
H	22.4	0.78	-6.77	-0.213	3.26	3.40

Table 4: Theoretical data including enhancement factors (EF) and properties of charge transfer (CT) states from calculations performed for halogen substitutions on benzenethiol in solvent

Functional Group	*Total EF (peaks between 500- 2000 cm^{-1})*	*HOMO-LUMO gap (eV)*	*Lowest CT Orbital (with 20% mixing) (eV)*	*Molecule Charge (q_e)*	*CT State peak (eV)*	
					To Ag	*From Ag*
m-F	459.4	0.81	-6.60	-0.317	3.22	2.60
m-Cl	460.1	0.81	-6.56	-0.325	2.94	2.62
m-Br	455.6	0.81	-6.52	-0.327	2.94	2.58
m-I	386.2	0.81	-6.97	-0.319	2.90	2.56
p-F	636.6	0.81	-5.78	-0.311	2.80	2.64
p-Cl	331.1	0.80	-6.75	-0.322	3.24	2.52
p-Br	282.8	0.80	-6.98	-0.325	2.78	2.52
p-I	183.8	0.81	-6.84	-0.314	3.04	2.56
H	458.0	0.81	-6.58	-0.286	2.82	2.56